POLITECNICO DI TORINO
Repository ISTITUZIONALE

Nonlinear system identification of a double-well Duffing oscillator with position-dependent friction

Original
Nonlinear system identification of a double-well Duffing oscillator with position-dependent friction / Zhu, R., Marchesiello, S., Anastasio, D., Jiang, D., Fei, Q.. - In: NONLINEAR DYNAMICS. - ISSN 0924-090X. - ELETTRONICO. - (2022). [10.1007/s11071-022-07346-1]

Availability:
This version is available at: 11583/2961756 since: 2022-04-21T12:16:46Z

Publisher:
Springer

Published
DOI:10.1007/s11071-022-07346-1

Terms of use:

This article is made available under terms and conditions as specified in the corresponding bibliographic description in the repository

Publisher copyright
Springer postprint/Author's Accepted Manuscript

This version of the article has been accepted for publication, after peer review (when applicable) and is subject to Springer Nature's AM terms of use, but is not the Version of Record and does not reflect post-acceptance improvements, or any corrections. The Version of Record is available online at: http://dx.doi.org/10.1007/s11071-022-07346-1

(Article begins on next page)

09 September 2026

Post-print version

Nonlinear system identification of a double-well Duffing oscillator with position-dependent friction

Rui Zhu[1], Stefano Marchesiello[2], Dario Anastasio[2], Dong Jiang[3], and Qingguo Fei [1]*

[1]School of Mechanical Engineering, Southeast University, Nanjing, China

[2]Dipartimento di Ingegneria Meccanica ed Aerospaziale, Politecnico di Torino, Torino, Italy

[3]School of Mechanical and Electronic Engineering, Nanjing Forestry University, Nanjing, China

https://doi.org/10.1007/s11071-022-07346-1

Cite as:

Zhu, R., Marchesiello, S., Anastasio, D. et al. Nonlinear system identification of a double-well Duffing oscillator with position-dependent friction. Nonlinear Dynanimcs (2022). https://doi.org/10.1007/s11071-022-07346-1.

Nonlinear system identification of a double-well Duffing oscillator with position-dependent friction

Rui Zhu[1], Stefano Marchesiello[2], Dario Anastasio[2], Dong Jiang[3], and Qingguo Fei[1]*

[1]*School of Mechanical Engineering, Southeast University, Nanjing, China*
[2]*Dipartimento di Ingegneria Meccanica ed Aerospaziale, Politecnico di Torino, Torino, Italy*
[3]*School of Mechanical and Electronic Engineering*, *Nanjing Forestry University, Nanjing, China*

Abstract: A double-well Duffing oscillator with nonlinear damping is identified in this paper, using the nonlinear subspace identification (NSI) technique in conjunction with a novel virtual input perturbation approach. This kind of system exhibits a negative stiffness characteristic, which has become popular in engineering applications such as vibration absorbers. The studied device exhibits strong nonlinear elastic and damping behaviors. In particular, the latter results in a very challenging identification, and the applicability of the proposed method to nonlinear damping is therefore discussed. In this context, the method is first tested considering simulations with quadratic friction. The experimental investigation is eventually undertaken considering a broadband random excitation, with a friction model depending on both velocity and displacement. Results show that NSI is capable of estimating the nonlinear model associated with stiffness and damping nonlinearities with a high level of confidence. This is particularly true in the case of complex nonlinear behaviors related to the double-well characteristics, using the proposed virtual input perturbation technique. This is confirmed also by the proposed experimental application and enlarges the range of applications of the NSI technique.

Keywords: double-well; Duffing; negative stiffness; nonlinear system identification; friction

1. Introduction

Historically, the dynamic features of nonlinear systems such as sub/super-harmonic resonances and chaotic solutions are responsible for undesired behaviors in real-life engineering applications [1]. However, the recent trend of design practice tends to use nonlinearity to improve the performance of engineering systems. Among the possible applications, typical examples include vibration isolation systems based on negative or quasi-zero stiffness elements [2,3] and energy harvesting [4–6]. The use of negative or quasi-zero stiffness elements as vibration isolators has considerably grown attention in material science and structural dynamics due to the amplified damping properties they bring [7]. This kind of devices are usually designed with discrete macroscopic elements, such as post-buckled beams and pre-compressed springs, to achieve the negative stiffness phase. Examples of this kind of application include: vehicle suspension guide mechanisms [8], devices to attenuate seismic vibrations [9,10] and vibration isolation of the vehicle seat [11]. On the microscopic side, negative-stiffness inclusions of ferro-elastic vanadium dioxide have been proposed in a pure tin matrix in [12]. A particular case is obtained when the negative stiffness approaches the “quasi-zero” value. This class of mechanisms is called quasi-zero-stiffness (QSZ) [13] and has the advantage of enhanced isolation capabilities without adding a linear stiffness contribution to the system. More details on the static and the dynamic behavior of QSZ mechanisms can be found in [14,15], while several applications are presented in [16–22].

Despite the mentioned recent applications, the concept of systems exhibiting a negative stiffness

* Corresponding author.
E-mail address: qgfei@seu.edu.cn

phase is decades older. Moon et al. [23] presented the experimental evidence for chaotic type non-periodic motions of a deterministic magnetoelastic oscillator called “negative stiffness system” in the late 70s, with a ferromagnetic beam buckled between two magnets. Systems with nonlinear features like this one are also referred to as double-well Duffing oscillators [24,25], with the negative stiffness effect coupled to a polynomial nonlinear characteristic. This oscillator exhibits two stable equilibrium positions plus an unstable one, and the oscillations can either be bounded around one stable point (in-well oscillations) or include all three positions (cross-well oscillations). In both cases, periodic oscillations can evolve to steady in-well or cross-well chaotic motions under external excitation [25]. This oscillator belongs therefore to the class of systems capable of exhibiting a chaotic behavior, a well-known phenomenon in several scientific areas [1,26,27].

On the experimental side, the rich nonlinear dynamics resulting from the presence of multiple equilibrium positions make the identification of this kind of systems really challenging. In this work, the nonlinear identification of double-well Duffing oscillator is pursued to extract a reliable model of its nonlinear characteristics from broadband random excitation measurements. In particular, the device is characterized by a double-well nature and a strong frictional behavior, resulting in a strong nonlinear behavior. A first attempt to identify the elastic nonlinear behavior of this device has been made in [28] using the nonlinear subspace identification (NSI) technique [29] and shifting the zero-reference of the system to overcome the negative linear stiffness issue. However, the identification of the nonlinear dissipation mechanisms of the structure has not been pursued at first. In [30], a first investigation of the frictional behavior of the device has been presented using the harmonic balance method in conjunction with a continuation technique. In this case, the analysis was restricted to a fixed frequency harmonic response and therefore not appropriate to extrapolate a predictive model.

The challenge in this work is instead on the simultaneous identification of stiffness and frictional nonlinearities using a single broadband measurement. The most important techniques available in the literature for nonlinear system identification of structural dynamics have been systematically reviewed in [31,32], but the existing identification methods mainly focus on nonlinear stiffness and less on identifying frictional nonlinearities or nonlinear damping. In real-life mechanical structures, friction is a complex nonlinear phenomenon that can take place in the “pre-sliding” or “sliding” regimes. Common examples of sliding friction are Coulomb-type and quadratic friction [33], and their identification from experimental measurements can be a challenging task, especially when other nonlinear sources are present in the structure under test. Worden et al. [34] introduced black box approaches to simulate the nonlinear dependence of pre-sliding friction and sliding friction, including neural networks, non-parametric models, and recurrent networks. In [35], the characterization of friction at the joints of the wing-payload substructure of an F-16 aircraft has been determined by using the restoring force surface [36] and wavelet transform [37] methods. An experimental investigation of a Coulomb friction oscillator under harmonic base excitation and joined base-wall excitation has been presented in [38].

Motivated by the above analysis, this paper further investigates the identification of a double-well Duffing oscillator with friction. The nonlinear subspace identification (NSI) method is further developed to consider such nonlinearity. The main contributions of this study lie in the following:

1. A new approach is presented to perform the identification of a double-well system with NSI. The approach is based on a virtual input perturbation to control the underlying-linear dynamics of the system.
2. Considering the effect of friction, the nonlinear subspace identification method is further developed, where nonlinear damping is regarded as an internal feedback force. The effectiveness of the method is first tested with numerical simulations.
3. A friction model is proposed based on the characteristics of the tested device and depending on both velocity and displacement.
4. The experimental study of the nonlinear negative system is conducted.

The proposed methodology is therefore valid to identify nonlinear systems that fits into the problem statement of NSI and that show a double-well characteristic or a complex frictional behavior.

The rest of this paper outline is as follows: section 2.1 introduces the model of the tested device. Section 2.2 discusses the problem statement based on NSI formulation with the input perturbation method. The identification strategy is tested in section 3 by simulating the response of the system with a friction contribution. Section 4 presents the experimental study and the results of the identification. Conclusions are eventually drawn in section 5.

2. Identification of a double-well Duffing oscillator with generalized nonlinear damping

2.1 Mathematical model

The device under test is composed of a U-shaped frame connected through rods to a central moving mass, as in figure 1. A bi-stable mechanism is achieved when the length of the rods is set so as to keep them under compression.

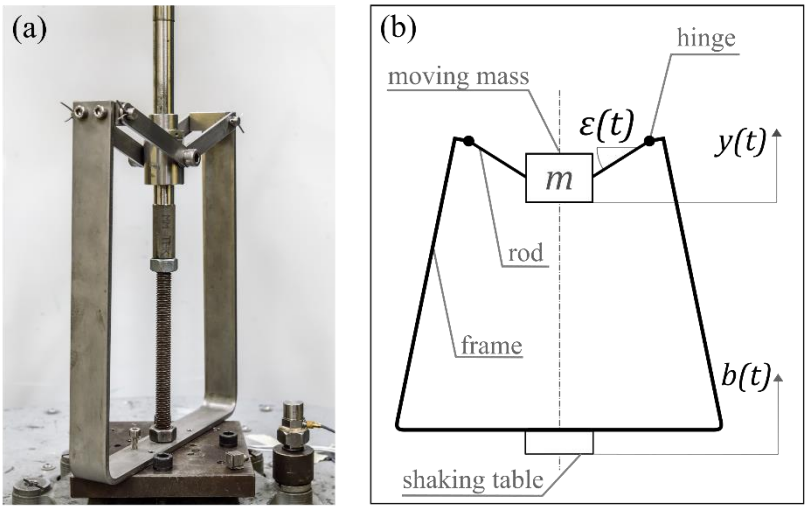

Figure 1: Photo of the oscillator system (a) and schematic representation (b).

The device is installed on a shaking table which exerts a displacement $b(t)$ on the structure. It is assumed that the inertia of the moving parts can be concentrated on one central point m, including the mass of the central bush and the equivalent inertia of the rods. The vertical movement of this point is described by the coordinate $y(t)$ and the rotation of the rods is expressed as ε. Since the bending elasticity of the frame is much higher than the axial elasticity of the rods, the latter are considered to be infinitely rigid.

Given the above considerations, the elastic force transmitted from half-frame to the moving point during its motion can be written as a function $p(\varepsilon)$ of the angle ε, as shown in figure 2. The dynamic equation of the system along the vertical direction can be written as

$$m\ddot{y}(t) + 2p\big(\varepsilon(t)\big)\sin\big(\varepsilon(t)\big) + mg = 0. \tag{1}$$

The relative motion $z(t)$ of the moving mass can be obtained as

$$z(t) = y(t) - b(t). \tag{2}$$

Then Eq. (1) can be expressed as

$$m\ddot{z}(t) + 2p\big(\varepsilon(t)\big)\sin\big(\varepsilon(t)\big) + mg = -m\ddot{b}(t), \tag{3}$$

where the external force is $f(t) = -m\ddot{b}(t)$.

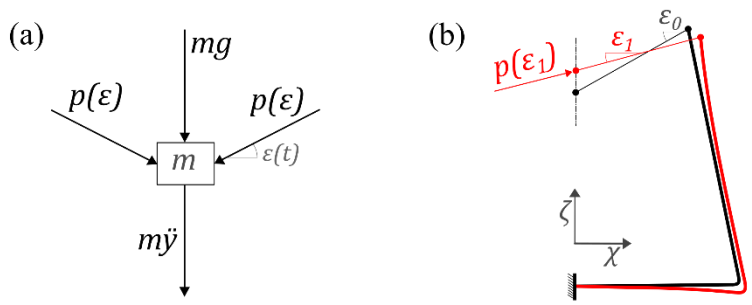

Figure 2: Force analysis (a) and model of the half-frame (b).

The analytic expression of $p(\varepsilon)$ can be determined by studying the flexibility of the half-frame, considered as two connected cantilever beams under bending stress. Also, a relationship between the angle $\varepsilon(t)$ and the position $z(t)$ can be derived as well. It is not the purpose of this work to analytically derive those quantities, but a qualitative representation of the vertical and horizontal components of $p(z)$ is depicted in figure 3 as a function of z.

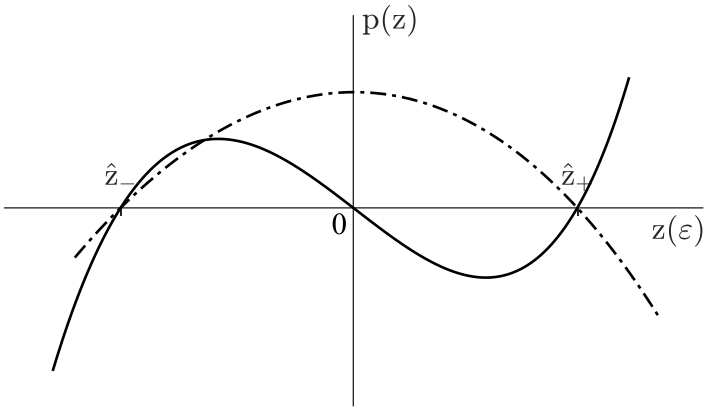

Figure 3: Qualitative graph of the force $p(z)$. Continuous black line: vertical component p_ζ; dashed-dotted black line: horizontal component p_χ.

The total vertical component p_ζ of p is defined as $p_\zeta = 2p(\varepsilon)\sin(\varepsilon)$, and it has three roots and crosses the origin with a negative slope. By adopting a polynomial expansion of degree 3, $p_\zeta(z)$ can be written as:

$$p_\zeta(z) = k_3 z^3 + k_2 z^2 - k_1 z, \tag{4}$$

where k_3 and k_2 are the nonlinear stiffness coefficients, and k_1 is the negative linear stiffness. Positive and negative roots of $p_\zeta(z)$ in figure 3 are respectively called $\hat{z}_+$ and $\hat{z}_-$.

Given the above considerations, the equation of motion along the vertical direction in the z variable can be expressed as

$$m\ddot{z} + \mathcal{D}(\dot{z}, z) + k_3 z^3 + k_2 z^2 - k_1 z + mg = f(t), \tag{5}$$

where a generalized damping force $\mathcal{D}(\dot{z}, z)$ is introduced. This force can be either linear or nonlinear and depending only on the velocity or also on the displacement. Eq. (5) has the form of a Duffing equation with negative linear stiffness.

Calling $\mathcal{K}(z)$ the elastic restoring force, it is expressed as

$$\mathcal{K}(z) = k_3 z^3 + k_2 z^2 - k_1 z + mg, \tag{6}$$

while the potential $\mathcal{U}(z)$ associated to $\mathcal{K}(z)$ can be defined as

$$\mathcal{U}(z) = \frac{1}{4}k_3 z^4 + \frac{1}{3}k_2 z^3 - \frac{1}{2}k_1 z^2 + mgz. \tag{7}$$

The equilibrium positions of the system are generally called z^* and can be obtained by setting $\mathcal{K}(z^*) = 0$. Two out of three locations represent a stable equilibrium, namely $z_{\pm}^*$, while the central position z_0^* is an unstable equilibrium point, as depicted in figure 4.

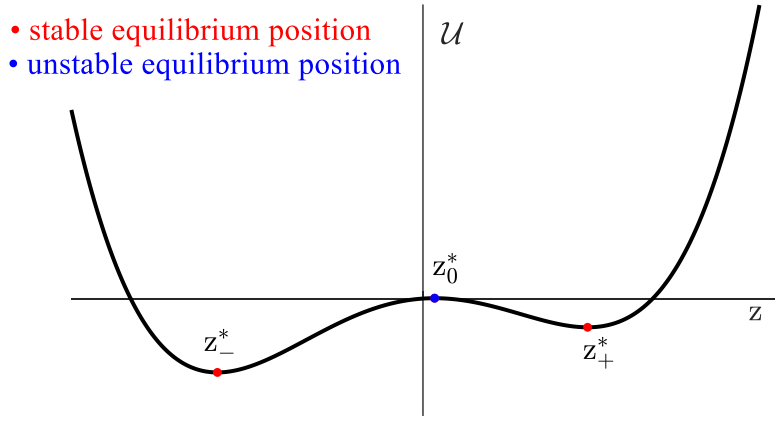

Figure 4: The potential of the system $\mathcal{U}(z)$.

It should be noted that the equilibrium positions of the system $z_{\pm}^*$ are not generally the same as the roots $\hat{z}_{\pm}$ of $p(z)$. This is because the latter does not account for the effects of gravity, which shifts the equilibrium positions.

The oscillations of the moving point are said to be "in-well" when the motion is bounded around one of the two stable equilibrium positions $z_{\pm}^*$. The associated linear natural frequency $\omega_{n,\pm}$ can be computed by

$$\omega_{n,\pm} = \sqrt{\frac{\mathcal{K}'(z_{\pm}^*)}{m}}, \tag{8}$$

where $\mathcal{K}'(z_{\pm}^*)$ is the first derivative of $\mathcal{K}(z)$ computed in z_-^* or z_+^*.

As for the horizontal component p_χ of p, this acts as a normal force with respect to the vertical movement of the mass. The force p_χ is maximum at $z = 0$ when the rods are at their maximum compression, and equal to zero at $\hat{z}_{\pm}$, as depicted in figure 3. By normalizing its maximum value to 1, the following conditions can be written:

$$\begin{cases} p_\chi(\hat{z}_-) &= 0 \\ p_\chi(\hat{z}_+) &= 0 \\ p_\chi(0) &= 1 \\ \left.\dfrac{dp_\chi}{dz}\right|_{z=0} &= 0 \end{cases} \tag{9}$$

Having a set of four conditions, the force p_χ can be expressed as a polynomial function with four coefficients $\alpha, \beta, \gamma, \delta$:

$$p_\chi(z) = \alpha z^3 + \beta z^2 + \gamma z + \delta. \tag{10}$$

The coefficients of Eq. (10) can be determined by applying the conditions of Eq. (9), yielding

$$\alpha = \frac{\hat{z}_-{}^3 - \hat{z}_+{}^3}{\hat{z}_-{}^2 - \hat{z}_+{}^2} - \hat{z}_+{}^3 - 1, \quad \beta = -\alpha\frac{\hat{z}_-{}^3 - \hat{z}_+{}^3}{\hat{z}_-{}^2 - \hat{z}_+{}^2}, \quad \gamma = 0, \quad \delta = 1. \tag{11}$$

It follows that the horizontal component of p is entirely described once the roots $\hat{z}_+$ are known. This relationship will be used as an a-priori information in Section 4 to perform the experimental identification of the structure under test.

2.2 System identification procedure with NSI via input perturbation

The main requirement of the nonlinear subspace identification technique is that the nonlinear system can be split into an underlying-linear part plus a nonlinear one. The former in particular must be a stable system, described by a linear FRF matrix $H(\omega)$. Consequently, this technique cannot be applied directly to the considered system, which exhibits a double-well nature.

A possible workaround has been presented in [28], and it consists in shifting the zero-reference to one of the stable equilibrium positions. This implicates the definition of a new displacement variable $x(t) = z - z_{\pm}^{*}$, such that the oscillations around its zero value are defined by a stable underlying-linear system. The main drawback of this approach is that it can be applied to both the equilibrium positions, leading to a double estimation of the coefficients of the nonlinear terms.

In this paper, a novel methodology is proposed which does not require the shifting of the zero-reference but it is based on a fictitious modification of the input force. Starting from Eq. (5), a linear elastic contribution $\tilde{k}_1 z$ can be added to both sides of the equation, yielding

$$m\ddot{z} + \mathcal{D}(\dot{z}, z) + k_3 z^3 + k_2 z^2 - k_1 z + \tilde{k}_1 z + mg = -m\ddot{b} + \tilde{k}_1 z. \tag{12}$$

Shifting the static value mg to the right and side of the equation and collecting the terms in z yields

$$m\ddot{z} + \mathcal{D}(\dot{z}, z) + k_3 z^3 + k_2 z^2 + \left(\tilde{k}_1 - k_1\right) z = -m\left(\ddot{b} + g\right) + \tilde{k}_1 z = \bar{f}(t). \tag{13}$$

If the choice of the linear stiffness $\tilde{k}_1$ is done such that

$$\bar{k}_1 = \tilde{k}_1 - k_1 > 0,$$

then the underlying-linear system described by Eq. (13) is stable and NSI can be applied. The new input force fed to NSI is the *perturbated* one $\bar{f}(t)$. Note that the value of $\tilde{k}_1$ can be either guessed by trial-and-error, i.e. until NSI gives a stable ULS in return, or by prior knowledge of the expected original linear (negative) stiffness. Also, the perturbation of the input force is only virtual and it does not require other experimental measurements.

As for the damping force $\mathcal{D}(\dot{z}, z)$, the only assumption needed is that it can be expressed as a linear viscous damping plus a sum of N_D nonlinear contributions, if any:

$$\mathcal{D}(\dot{z}, z) = c_v \dot{z} + \sum_{j=1}^{N_D} c_j g_j(\dot{z}, z). \tag{14}$$

The coefficient c_v is the linear viscous damping term, while g_j is the j^{th} nonlinear basis function related to a nonlinear damping term.

By moving the nonlinear terms of Eq. (13) to the right-hand side one obtains:

$$m\ddot{z} + c_v \dot{z} + \bar{k}_1 z = \bar{f}(t) + \underbrace{\left(-k_3 z^3 - k_2 z^2 - \sum_{j=1}^{N_D} c_j g_j\right)}_{f_{nl}(t)} = \bar{f}(t) + f_{nl}(t). \tag{15}$$

The system can be viewed as an underlying-linear system subjected to the external force $\bar{f}(t)$ and to a set of internal feedback forces due to nonlinearities $f_{nl}(t)$, as shown in figure 5.

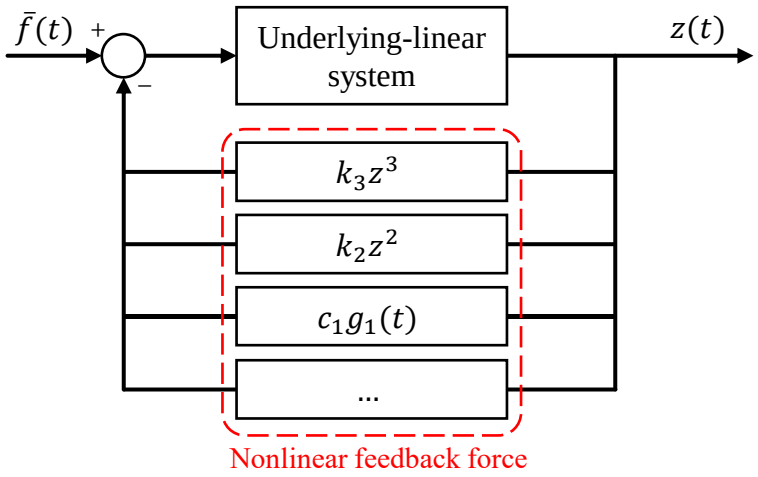

Figure 5: Closed-loop representation of the nonlinear vibrating system.

Assuming that the measurements concern displacements only, the state-space formulation of the equation can be expressed by Eq. (16)~(17).

$$\begin{Bmatrix} \dot{z} \\ \ddot{z} \end{Bmatrix} = \underbrace{\begin{bmatrix} 0 & 1 \\ -\frac{\bar{k}_1}{m} & -\frac{c_v}{m} \end{bmatrix}}_{A_c} \begin{Bmatrix} z \\ \dot{z} \end{Bmatrix} + \underbrace{\begin{bmatrix} 0 & 0 & 0 & 0 & 0 & \dots \\ \frac{1}{m} & \frac{k_3}{m} & \frac{k_2}{m} & \frac{c_1}{m} & \frac{c_2}{m} & \dots \end{bmatrix}}_{B_c} \begin{Bmatrix} \bar{f}(t) \\ -z^3 \\ -z^2 \\ -g_1(t) \\ -g_2(t) \\ \dots \end{Bmatrix} \tag{16}$$

$$z = \underbrace{[1 \quad 0]}_{C} \begin{Bmatrix} z \\ \dot{z} \end{Bmatrix} + \underbrace{[0 \quad 0 \quad 0 \quad 0 \quad 0 \quad \dots]}_{D} \begin{Bmatrix} \bar{f}(t) \\ -z^3 \\ -z^2 \\ -g_1(t) \\ -g_2(t) \\ \dots \end{Bmatrix} \tag{17}$$

The modal parameters of the underlying-linear system can be determined by solving the eigenvalue problem of the dynamical matrix A_c. It is worth highlighting that the identification simply fails if the value of $\tilde{k}_1$ is chosen to be lower than k_1. Considering the eigenvalue decomposition of A_c:

$$A_c = \psi \Lambda_c \psi^{-1}, \tag{18}$$

the diagonal matrix Λ_c will not return complex-conjugate eigenvalues in such scenario, but real values instead. This gives an intuitive methodology to choose the value of $\tilde{k}_1$.

Based on the authors' previous work about the nonlinear subspace identification, the "extended" frequency response function (FRF) matrix is expressed as

$$H_E(\omega) = D + C(i\omega I - A_c)^{-1} B_c, \tag{19}$$

where ω is the angular frequency and $i = \sqrt{-1}$. It is worth noticing that the formulation of Eq. (19) is a standard result in linear systems theory, although the meaning of the terms is in this case different. To better clarify this, the matrices in Eq. (16) and Eq. (17) can be substituted into Eq. (19), obtaining

$$H_E(\omega) = [\bar{H} \quad \bar{H}k_3 \quad \bar{H}k_2 \quad \bar{H}c_1 \quad \bar{H}c_2 \quad \dots], \tag{20}$$

where $\bar{H}$ is the underlying-linear receptance matrix of the perturbed system. The nonlinear coefficients can be estimated based on Eq. (20), resulting in frequency-dependent and complex-valued quantities [29]. As known, the true nonlinear coefficients are real numbers. Therefore, the imaginary part of the estimated counterparts should be zero and the real part should not depend on the frequency. However, this is not

generally the case due to the existence of noise and nonlinear modelling errors. The average ratio $E[\Re/\Im]$ between real and imaginary parts can be taken as an indicator to evaluate the goodness of the identification in real situations. The larger the ratio is, the better the recognition result will be; conversely, the smaller the ratio is, the worse the estimation will be. The latter case can be considered as symptomatic of a weak participation of the associated nonlinearity to the system response, or of a high noise corruption. The flow-chart of the identification procedure is depicted in figure 6.

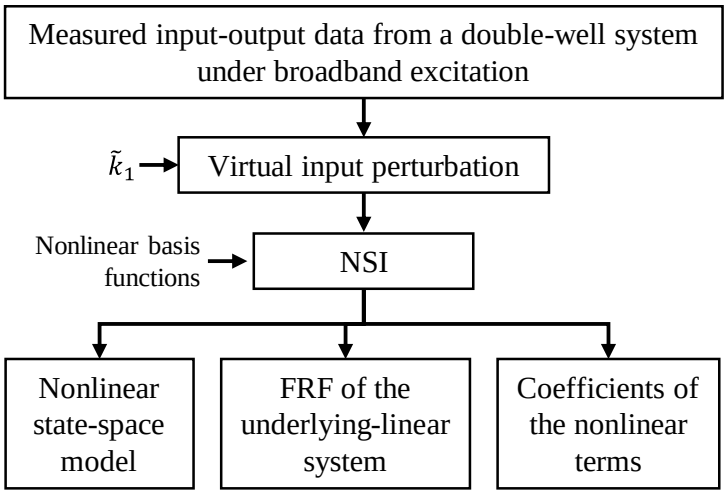

Figure 6: Flow-chart of the virtual input pertubation approach with NSI.

3. Numerical application

A numerical example is presented in the following to test the capability of the nonlinear identification scheme of estimating the underlying-linear FRF and the nonlinear parameters. The system concerns a double-well Duffing oscillator with linear viscous damping and quadratic friction. The dynamic equation of motion reads

$$m\ddot{z} + c_v\dot{z} + \mu\,\mathrm{sign}(\dot{z})\dot{z}^2 + k_3z^3 + k_2z^2 - k_1z + mg = f(t). \tag{21}$$

The system parameters are: $m = 0.2\,\mathrm{kg}, k_3 = 10^6\,\frac{\mathrm{N}}{\mathrm{m}^3}, k_2 = 5\times10^3\,\frac{\mathrm{N}}{\mathrm{m}^2}, k_1 = 5\times10^2\,\frac{\mathrm{N}}{\mathrm{m}}, c_v = 1\,\frac{\mathrm{Ns}}{\mathrm{m}}, \mu = 5\,\frac{\mathrm{Ns}^2}{\mathrm{m}^2}$.

The forcing function $f(t)$ is a zero-mean Gaussian random input, whose root-mean-square (RMS) value is $50\ \mathrm{N}$. These values have been selected to ensure a strong nonlinear response, which is calculated by Runge-Kutta fourth-order method with a sampling frequency of $2048\ \mathrm{Hz}$ and an acquisition length of $60\ \mathrm{s}$. Furthermore, the generated outputs are corrupted with zero-mean Gaussian noise in the measure of 2% of the signal standard deviation. The displacement $z(t)$ is depicted in figure 7.

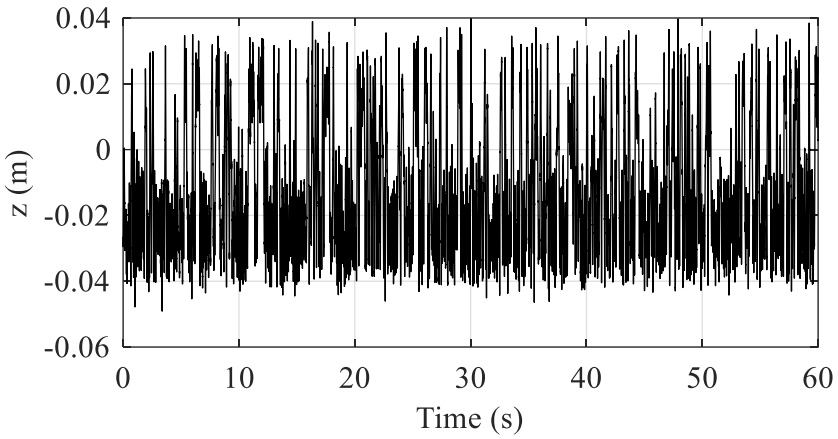

Figure 7: Simulated displacement of the system with quadratic friction.

The restoring force and the corresponding potential are shown in figure 8. Two out of three positions represent a stable equilibrium, namely $z_-^* = -0.027$ m and $z_+^* = 0.017$ m, while the central position $z_0^* = 0.004$ m is an unstable equilibrium point.

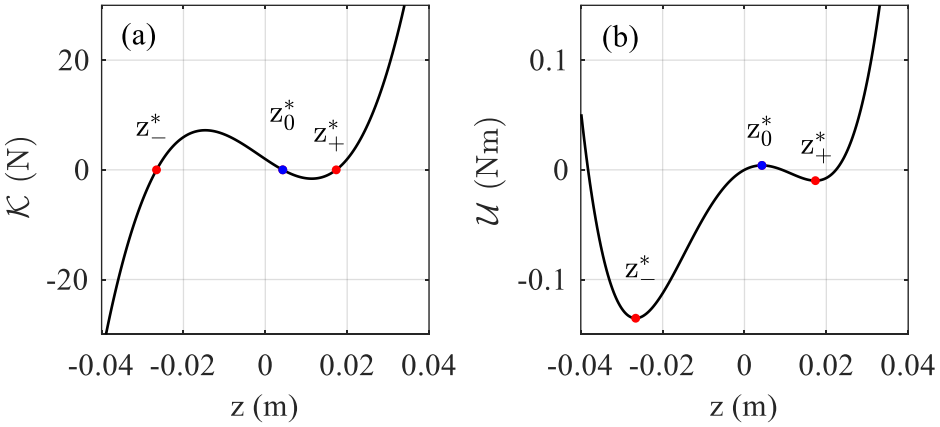

Figure 8: Restoring force (a) and potential (b) of the simulated system. The stable equilibrium positions are marked in red, while the unstable position is marked in blue.

3.1 Nonlinear system identification via zero-reference shift

The method proposed in [28] is here applied to perform the nonlinear system identification with NSI. This approach requires a zero-reference shift, and implies that the two stable equilibrium positions of the system correspond to two underlying-linear systems mutually exclusive. Therefore, the identification should be repeated twice, shifting the zero-reference to both equilibrium positions. The stable equilibrium position z_-^* is considered first, and a new displacement variable $x = z - z_-^*$ is adopted to perform the identification in NSI. The procedure is then repeated for the position z_+^*.

The singular value plot is presented in figure 9, where a clear jump between model orders two and three can be noted. NSI is then applied considering a model order $n = 2$.

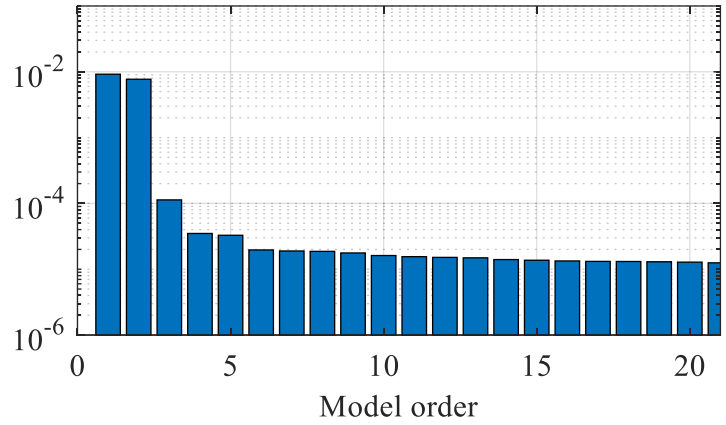

Figure 9: Singular value plot with 2% measurement error and zero-reference shift approach.

Figure 10 shows the underlying estimated FRF $H(\omega)$ obtained with NSI compared against the theoretical one. Results show that the underlying linear FRF is in very good agreement with the true value.

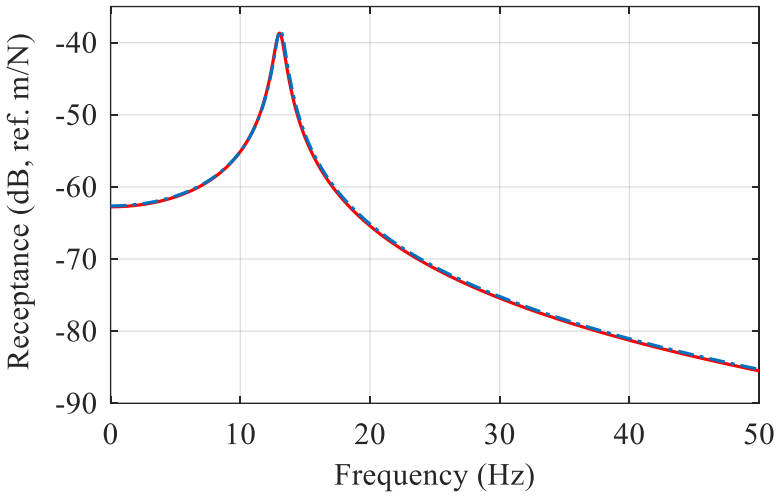

Figure 10: Underlying-linear FRF of the oscillations around the stable equilibrium position z_-^*. Red line: true FRF; dashed-dotted blue line: estimated FRF using NSI with zero-reference shift.

The estimated modal parameters of the two underlying-linear systems are reported in table 1 considering both reference positions. Errors are below 1% for the frequencies and 3% for the damping ratios, confirming the goodness of the identification.

Table 1: Modal parameters of the two underlying-linear systems estimated using NSI with zero-reference shift.

Reference position	Natural frequency (Hz)			Damping ratio (%)		
	Exact	Estimated	Error %	Exact	Estimated	Error %
z_-^*	13.10	13.07	0.16	3.04	3.09	1.88
z_+^*	8.52	8.49	0.36	4.67	4.78	2.36

The coefficients of the nonlinear basis functions are also estimated and shown in figure 11 as frequency-dependent quantities for the reference position z_-^*. Similar results are obtained with the positive reference position z_+^*, and a summary of the estimated coefficients is listed in table 2. As shown in figure 11, the imaginary parts of the coefficients are orders of magnitudes lower with respect to the real parts, and the estimated parameters have good stability with respect to the frequency values. The

maximum error of the nonlinear parameters is 0.68%.

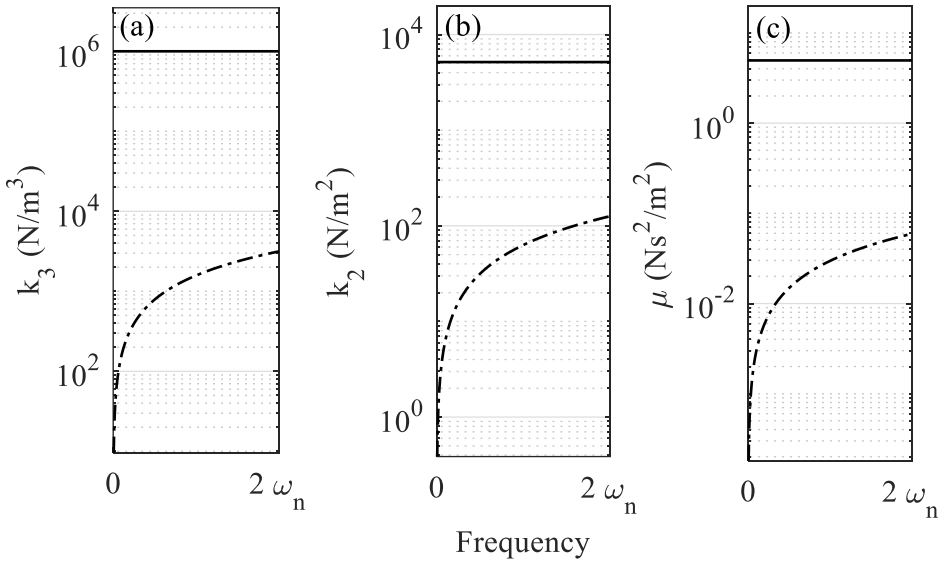

Figure 11: Real (black lines) and imaginary (dashed-dotted lines) parts of the estimated coefficients using NSI with zero-reference shift and reference position z_-^*. Y-axis is in logarithmic scales.

Table 2: Estimated parameters and relative errors using NSI with zero-reference shift.

Parameter	Exact value	Estimated parameters			
		Reference position z_-^*	Error %	Reference position z_+^*	Error %
k_3	1×10^6	9.998×10^5	0.02	9.996×10^5	0.04
k_2	5×10^3	5.034×10^3	0.68	4.987×10^3	0.24
k_1	-500	-502	0.45	-503	0.66
μ	5	4.98	0.37	4.97	0.61

3.2 Nonlinear system identification via input perturbation

The nonlinear identification strategy described in section 2.2 is here tested on the same numerical example previously proposed and using the same dataset. The input forcing function $f(t)$ is then perturbated according to Eq. (13) considering a linear fictitious stiffness $\tilde{k}_1$ and the static contribution mg.The new input $\bar{f}(t)$ is then obtained as

$$\bar{f}(t) = f(t) + \tilde{k}_1 z - mg.$$

To test the methodology, the identification is first performed with a value of $\tilde{k}_1 = 400$ N/m, which does not give a stable ULS in return. In this case, the estimated eigenvalue matrix Λ_c with model order 2 equals to

$$\Lambda_c|_{\tilde{k}_1=400} = \begin{bmatrix} 19.33 & 0 \\ 0 & -24.43 \end{bmatrix},$$

which as expected contains real-valued entries. Instead, by choosing $\tilde{k}_1 = 600$ N/m the identification succeeds and a stable ULS is retrieved. The estimated eigenvalue matrix is in this case:

$$\Lambda_c|_{\tilde{k}_1=600} = \begin{bmatrix} -2.54 + 22.36i & 0 \\ 0 & -2.54 - 22.36i \end{bmatrix}.$$

The singular value plot is presented in figure 12, where a clear jump between model orders two and three can be noted. NSI is then applied considering a model order $n = 2$ also in this case.

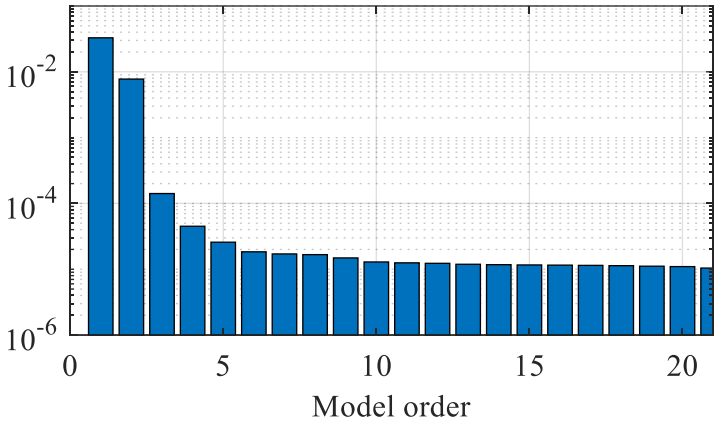

Figure 12: Singular value plot with 2% measurement error and input perturbation approach.

Note that with this approach the identified underlying-linear system is not the "true" one, but the perturbed one. Instead, the coefficients of the nonlinear terms are directly estimated, and depicted in figure 13. The ratio $E[\Re/\Im]$ between real and imaginary parts remains very high, confirming the goodness of the identification. A summary of the estimated coefficients is listed in table 3.

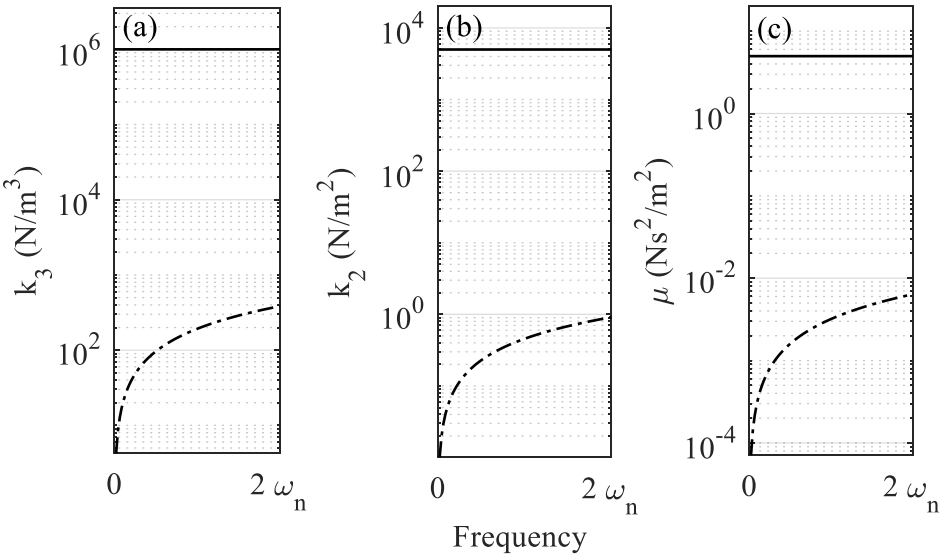

Figure 13: Real (black lines) and imaginary (dashed-dotted lines) parts of the estimated coefficients using NSI with input perturbation. Y-axis is in logarithmic scales.

Table 3: Estimated parameters and relative errors using NSI with input perturbation.

Parameter	Exact value	Estimated parameters	
		NSI with input perturbation	Error %
k_3	1×10^6	9.977×10^5	0.23
k_2	5×10^3	4.998×10^3	0.22
k_1	-500	-498	0.26
μ	5	4.98	0.37

Once the nonlinear parameters have been estimated, the restoring force of the system can be computed. The result is depicted in figure 14 and compared with the theoretical one. Note that the equilibrium positions of the system in this case are not a prior knowledge and can be estimated from the identified restoring force. The estimated values are $-0.0265\,\mathrm{m}, 0.0043\,\mathrm{m}$ and $0.0173\,\mathrm{m}$, with a maximum error of 0.3% with respect to the true ones.

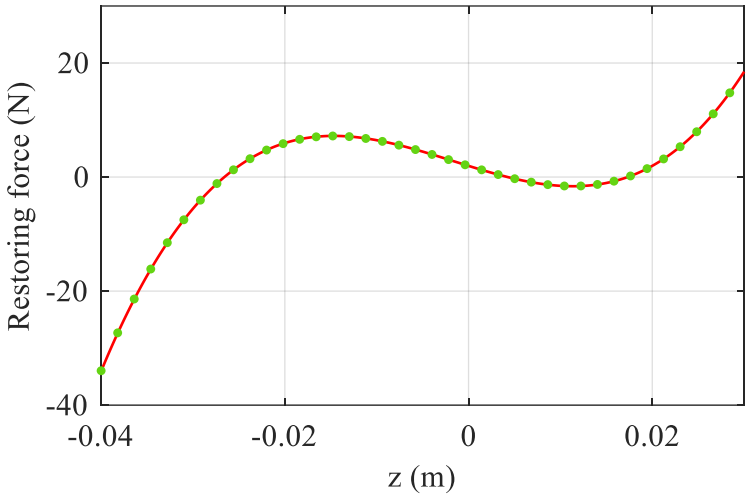

Figure 14: Theoretical restoring force (red line) and identified one (green dots) using NSI with input perturbation.

The natural frequencies of the oscillations around the two stable equilibrium positions are eventually obtained from the identified restoring force using Eq. (8). The associated damping ratios can be estimated starting from the identified state-space model of the perturbed system. Calling $\bar{\zeta}$ the estimated damping ratio, and $\bar{\omega}_n$ the estimated natural frequency of the perturbed system, the damping ratios $\zeta_\pm$ related to the two equilibrium positions can be obtained imposing the invariance of the linear viscous damping coefficient $c_v = 2\bar{\zeta}m\bar{\omega}_n = 2\zeta_\pm m\omega_{n,\pm}$ between true and perturbed system, yielding

$$\zeta_\pm = \bar{\zeta}\frac{\bar{\omega}_n}{\omega_{n,\pm}}. \tag{22}$$

Results are listed in table 4 and show a very good agreement, with errors below 1% for the natural frequencies and 2% for the damping ratios.

Table 4: Modal parameters of the two underlying-linear systems estimated using NSI with input perturbation.

Reference position	Natural frequency (Hz)			Damping ratio (%)		
	Exact	Estimated	Error %	Exact	Estimated	Error %
z_-^*	13.10	13.08	0.10	3.04	3.09	1.76
z_+^*	8.52	8.50	0.23	4.67	4.76	1.89

As a final product of the identification, the underlying estimated FRF $H(\omega)$ is depicted in figure 15 and compared against both the theoretical one and the previously identified one. In particular, the FRFs estimated with NSI using both approaches are practically overlapped, and very close to the theoretical one.

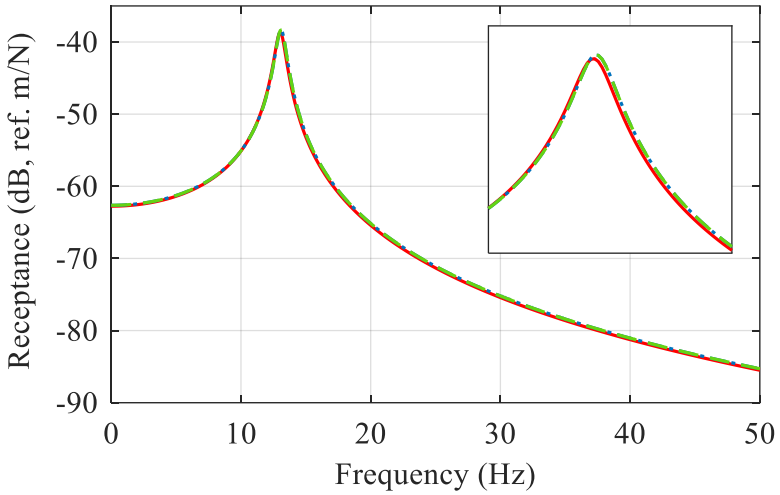

Figure 15: Underlying-linear FRF of the oscillations around the stable equilibrium position z_-^*. Red line: true FRF; dashed-dotted blue line: estimated FRF using NSI with zero-reference shift; dashed green line: estimated FRF using NSI with input perturbation.

4. Experimental study

The experimental application considering a double-well oscillator is conducted in this section. Two photos of the experimental setup are depicted in figure 16 showing the stable equilibrium positions of the device. The system is excited with a shaking table providing a random excitation, whose RMS value is chosen so as to obtain a cross-well motion. The acceleration of the base $\ddot{b}(t)$ is measured using an accelerometer, while the displacement of the moving point and its acceleration are measured using a laser vibrometer and an accelerometer respectively. The sampling frequency is 512 Hz, and the acquisition length is $t = 120$ s.

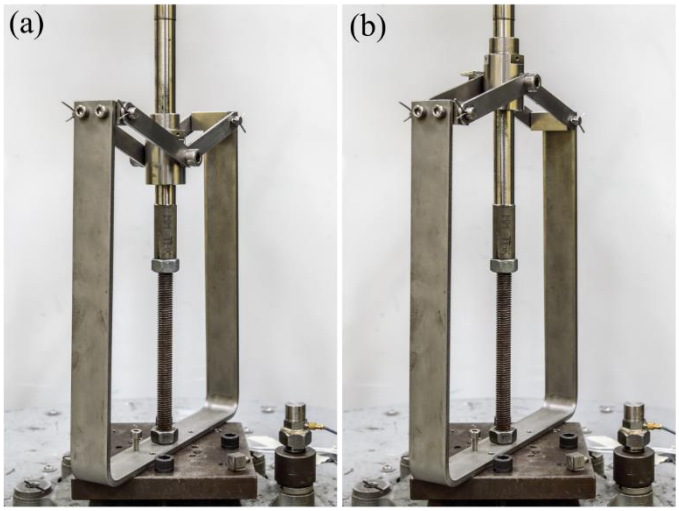

Figure 16: Experimental setup. (a) Negative equilibrium position; (b) positive equilibrium position.

The response signal is represented in figure 17(a), where repeated crossings between negative and positive values can be observed. The statistical distribution of $z(t)$ is depicted in figure 17(b) to highlight the asymmetric behavior of the device. The equilibrium positions are obtained in this case from a static measure and they are equal to $z_-^* = -0.030$ m and $z_+^* = 0.024$ m. Generally, methods exist to estimate equilibria from time series if needed, e.g. [39].

Based on the theoretical analysis of section 2, the equation of motion of the moving point along the vertical direction can be written as

$$m\ddot{z} + c_v\dot{z} + \mathcal{D}_{nl}(\dot{z}, z) + k_3z^3 + k_2z^2 - k_1z + mg = f(t), \tag{23}$$

where the damping force is expressed as the sum of a linear term $c_v\dot{z}$ and a nonlinear function $\mathcal{D}_{nl}(\dot{z}, z)$. For this experimental system, the nonlinear damping form is quite complex and difficult to determine. Nevertheless, it has been shown in [28] that it plays an important role in the system response, while in [30] its dependency on both the vertical position and the velocity of the moving point has been investigated considering harmonic measurements. This result is in accordance with the theoretical analysis of section 2, where it has been highlighted how the horizontal component p_χ of p is acting as a normal force with respect to the vertical movement of the mass.

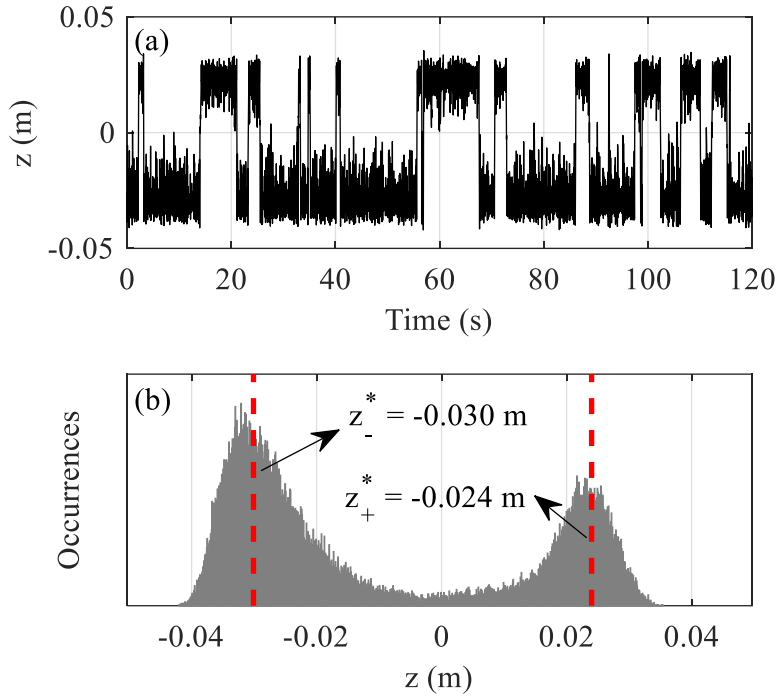

Figure 17: Random test. (a) Time history of the displacement; (b) Statistical distribution of the displacement. Dashed red lines indicate the equilibrium positions (static measure).

Since there is no prior knowledge about the dependency on the velocity of the nonlinear damping form, a common power damping law [40,41] is considered in the identification process:

$$\mathcal{D}_{nl}(\dot{z}, z) = \sum_{j=0}^{n_D} c_j \text{sign}(\dot{z})\dot{z}^j \cdot |\alpha z^3 + \beta z^2 + \gamma z + \delta|. \tag{24}$$

The nonlinear damping force in Eq. (24) is a sum of $n_D + 1$ terms, whose dependency on the position is associated to the horizontal force p_χ of Eq. (10). It should be noted that the absolute value of p_χ is considered, to keep the normal force positive and let the $\text{sign}(\cdot)$ function to determine the sign of each contribution. Also, the summation starts from zero to account for the Coulomb friction contribution $c_0\text{sign}(\dot{z})$. The formulation of Eq. (24) allows for the identification method to properly weight the different contributions, guaranteeing at the same time a good amount of flexibility. It is worth reminding that the coefficients α, β, γ and δ are completely defined provided that the roots $\hat{z}_\pm$ of p_ζ are known, as in Eq. (11).

Given the above considerations, NSI is applied to the experimental data using the input perturbation method and with the following set of nonlinear basis functions: z^3; z^2; $\sum_{j=0}^{n_D} \text{sign}(\dot{z})\dot{z}^j|p_\chi|$, $n_D = 3$.

The linear stiffness $\tilde{k}_1$ is selected iteratively with steps of $100\ \text{N/m}$ until a stable ULS is retrieved in NSI, that is for the value $\tilde{k}_1 = 600\ \text{N/m}$.

The singular value plot is depicted in figure 18, and the model order is set to $n = 2$, corresponding to the highest jump.

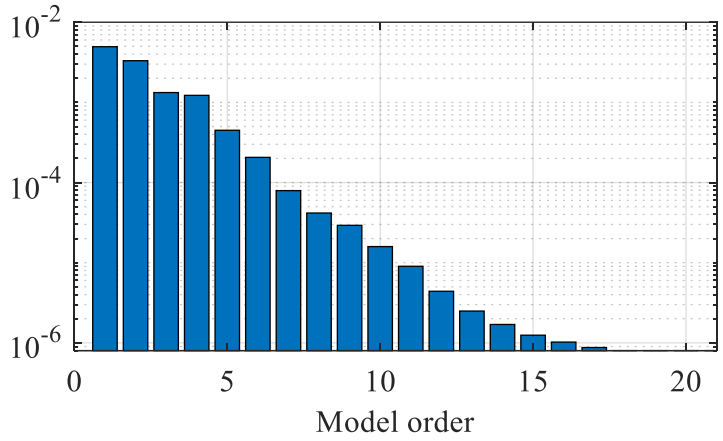

Figure 18: Singular value plot, experimental data.

The estimated coefficients are depicted in figure 19. Results show that the real part of the parameters keeps a horizontal line and does not depend on the frequency, verifying the effectiveness and stability of NSI.

The imaginary parts of the coefficients are always lower than the real parts, but the distance is generally reduced for the damping-related coefficients, indicating that the identified model structure is still affected by a combination of nonlinear modelling errors and noise. The average ratio between real and imaginary parts $E[\Re/\Im]$ is in any case at least equal to one order of magnitude. The complete list of the estimated coefficients is reported in table 5.

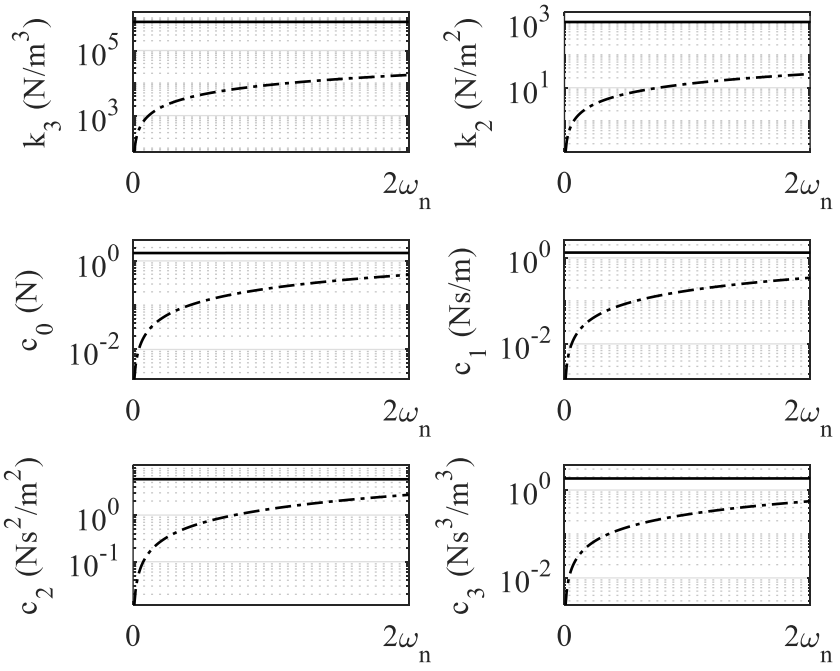

Figure 19: Real (black lines) and imaginary (dashed-dotted lines) parts of the identified coefficients using NSI with input perturbation. Y-axis is in logarithmic scales.

Table 5: Estimated parameters using NSI with input perturbation.

Parameter	k_3 (N/m^3)	k_2 (N/m^3)	c_0 (N)	c_1 (Ns/m)	c_2 (Ns^2/m^2)	c_3 (Ns^3/m^3)
Estimated value	7.57 ×10^5	9.86 ×10^2	1.51	-1.32	-5.86	1.84
$E[\Re/\Im]$	198	175	14	17	11	15

As for the linear part of the system, the same steps previously discussed are here applied to estimate the modal parameters associated to the oscillations around the two stable equilibrium positions. Results are listed in table 6. Also, the estimated linear (negative) stiffness value is $k_1 = -565$ N/m.

Table 6: Modal parameters of the two underlying-linear systems estimated using NSI with input perturbation.

Reference position	Natural frequency (Hz)	Damping ratio (%)
z_-^*	11.75	10.9
z_+^*	8.77	14.6

Eventually, the restoring surface $\mathcal{R}(z,\dot{z})$ is assembled from the identified coefficients as in Eq. (25), and compared with the experimental one $\mathcal{R}_e(z,\dot{z})$ to validate the identified model structure:

$$\mathcal{R}(z,\dot{z}) = \mathcal{K}(z) + \mathcal{D}(z,\dot{z}) = f(t) - m\ddot{z}. \tag{25}$$

The validation can be performed by defining the percentage RMS residual ϵ as

$$\epsilon = 100\frac{\mathrm{RMS}[\mathcal{R}(z,\dot{z}) - \mathcal{R}_e(z,\dot{z})]}{\mathrm{RMS}[\mathcal{R}_e(z,\dot{z})]}. \tag{26}$$

The residual in this case is equal to 4.42 %. It is worth noticing that when the identification is performed without nonlinear damping basis functions (i.e., only considering cubic and quadratic stiffness) the residual increases to 8.38 %, highlighting the importance of considering the nonlinear damping terms in the structure under test. The experimental and estimated restoring surface plots are depicted in figure 20.

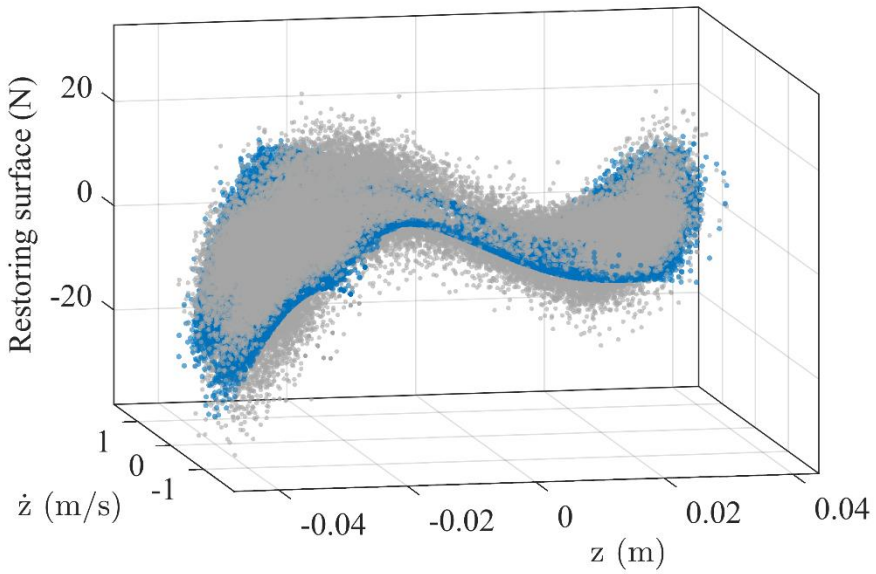

Figure 20: Experimental restoring surface $\mathcal{R}_e$ (grey dots) and estimated one $\mathcal{R}$ (blue dots).

The restoring force $\mathcal{K}(z)$ is eventually depicted in figure 21 together with three snapshots of the damping force $\mathcal{D}(z,\dot{z})$ in three different positions. The experimental counterparts are also shown,

obtained by properly slicing the experimental restoring surface $\mathcal{R}_e$.

The stable equilibrium positions $z_{\pm}^*$ can also be estimated from the identified restoring force and compared with the measured one. The comparison is reported in table 7, where a particularly low error can be appreciated, as a further confirmation of the goodness of the identification.

Table 7: Measured and estimated stable equilibrium positions.

Equilibrium position	Measured (m)	Estimated (m)	Error (%)
z_-^*	-0.030	-0.029972	-0.42
z_+^*	+0.024	+0.023984	0.06

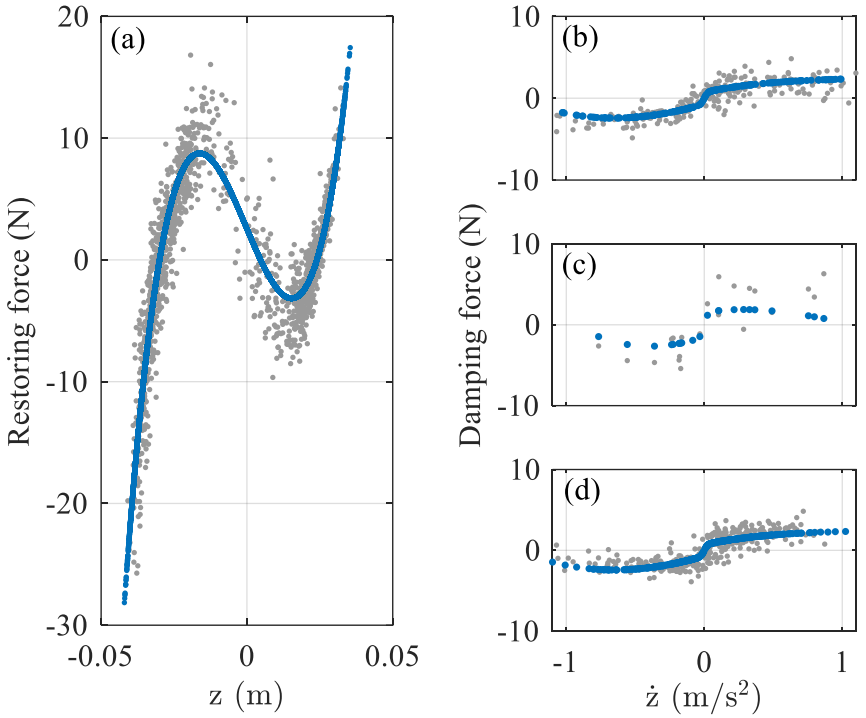

Figure 21: Identification of the restoring and damping forces. Grey dots: experimental points; blue dots: identified points. (a) Restoring force; (b) Damping force around $z = -0.02$ m; (c) Damping force around $z = 0$ m; (d) Damping force around $z = +0.02$ m.

The single RMS contributions to the identified restoring surface are depicted in figure 22. As expected, the major contributions come from the elastic terms, and in particular from the linear (negative) stiffness and the cubic one. As for the damping terms, the linear viscous term is predominant, followed by Coulomb and quadratic friction. The odd-exponent terms of the nonlinear damping force seem to give minor contributions.

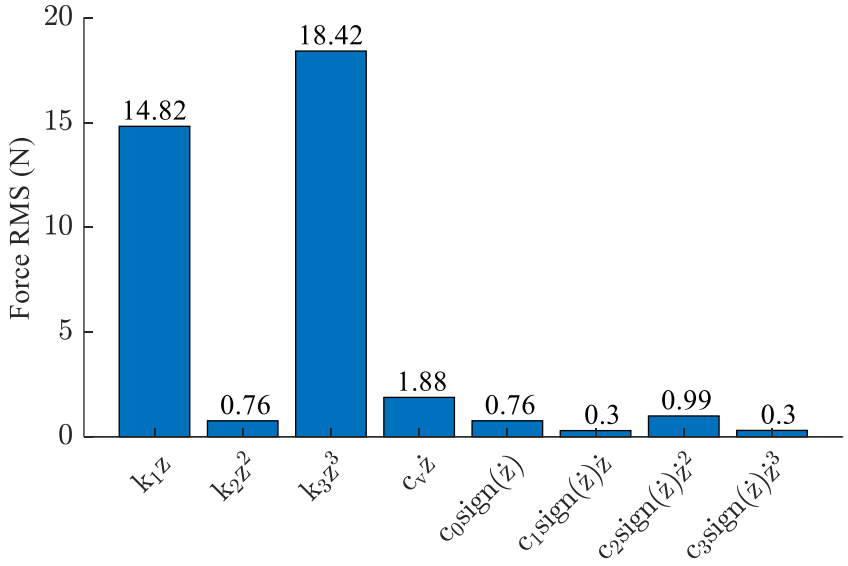

Figure 22: Single RMS contributions to the identified restoring surface.

5. Conclusion

This paper presents the experimental identification of a double-well oscillator system with nonlinear position-dependent damping. The parameter evaluation of the system has been introduced based on the nonlinear subspace identification method (NSI). In particular, a novel approach has been present based on a virtual input perturbation, to control the underlying-linear dynamics of the structure under test. The methodology has been tested first on a numerical example, and eventually considering an experimental application. The latter case results in a particularly challenging identification since the nonlinearity is strongly present in both stiffness and damping terms. The former is responsible for the cross-well motion and the negative linear stiffness contribution, while the latter depends on both velocity and displacement. The main conclusions are drawn as follows:

1. The so-called input perturbation approach in conjunction with NSI has proven to be a powerful method to identify nonlinear vibrating structures. The main advantage is the capability of controlling the underlying-linear dynamics of the system to ease the identification of the nonlinear part, without physically acting on the structure. Future studies might exploit the capability of this approach, which has been limited to a linear elastic perturbation in this work.
2. The effect of friction has been investigated. In the case of noise, the nonlinear coefficients associated to both stiffness and damping nonlinearities can be effectively identified by the proposed method, provided that they are properly excited by the input forcing function.
3. Experimental tests of a negative stiffness oscillator have been conducted and the identification performed. The friction model related to displacement and velocity has been identified by NSI, showing that this technique can be used to identify complex nonlinear basis functions depending on both velocity and displacement.

Acknowledgments This research work is supported by the National Natural Science Foundation of China (11602112 and 11572086), the Postgraduate Research and Practice Innovation Program of Jiangsu Province (KYCX19_0062), the Jiangsu Natural Science Foundation (BK20170022), and the Scientific Research Foundation of the Graduate School of Southeast University (YBPY2003).

Compliance with ethical standards

Conflict of interest The authors declare that they have no conflict of interest concerning the publication of this manuscript.

References

[1] S.H. Strogatz, Nonlinear Dynamics and Chaos, CRC Press, 2018. https://doi.org/10.1201/9780429492563.

[2] Z.Q. Lu, D. Wu, H. Ding, L.Q. Chen, Vibration isolation and energy harvesting integrated in a Stewart platform with high static and low dynamic stiffness, Applied Mathematical Modelling. 89 (2021). https://doi.org/10.1016/j.apm.2020.07.060.

[3] Z.Q. Lu, D.H. Gu, H. Ding, W. Lacarbonara, L.Q. Chen, Nonlinear vibration isolation via a circular ring, Mechanical Systems and Signal Processing. 136 (2020). https://doi.org/10.1016/j.ymssp.2019.106490.

[4] H. Ding, L.Q. Chen, Designs, analysis, and applications of nonlinear energy sinks, Nonlinear Dynamics. 100 (2020). https://doi.org/10.1007/s11071-020-05724-1.

[5] T. Yuan, J. Yang, L.Q. Chen, Nonlinear characteristic of a circular composite plate energy harvester: experiments and simulations, Nonlinear Dynamics. 90 (2017). https://doi.org/10.1007/s11071-017-3815-4.

[6] L.Q. Chen, Y.Q. Tang, J.W. Zu, Nonlinear transverse vibration of axially accelerating strings with exact internal resonances and longitudinally varying tensions, Nonlinear Dynamics. 76 (2014). https://doi.org/10.1007/s11071-013-1220-1.

[7] I. Antoniadis, D. Chronopoulos, V. Spitas, D. Koulocheris, Hyper-damping properties of a stiff and stable linear oscillator with a negative stiffness element, Journal of Sound and Vibration. 346 (2015) 37–52. https://doi.org/10.1016/j.jsv.2015.02.028.

[8] C.M. Lee, V.N. Goverdovskiy, A.I. Temnikov, Design of springs with “negative” stiffness to improve vehicle driver vibration isolation, Journal of Sound and Vibration. 302 (2007) 865–874. https://doi.org/10.1016/j.jsv.2006.12.024.

[9] A.A. Sarlis, D.T.R. Pasala, M.C. Constantinou, A.M. Reinhorn, S. Nagarajaiah, D.P. Taylor, Negative Stiffness Device for Seismic Protection of Structures, Journal of Structural Engineering. 139 (2013). https://doi.org/10.1061/(asce)st.1943-541x.0000616.

[10] H. Iemura, M.H. Pradono, Advances in the development of pseudo-negative-stiffness dampers for seismic response control, Structural Control and Health Monitoring. 16 (2009). https://doi.org/10.1002/stc.345.

[11] T.D. Le, K.K. Ahn, A vibration isolation system in low frequency excitation region using negative stiffness structure for vehicle seat, Journal of Sound and Vibration. 330 (2011) 6311–6335. https://doi.org/10.1016/j.jsv.2011.07.039.

[12] R.S. Lakes, Extreme damping in composite materials with a negative stiffness phase, Physical Review Letters. 86 (2001) 2897–2900. https://doi.org/10.1103/PhysRevLett.86.2897.

[13] J.Z. Zhang, D. Li, M.J. Chen, S. Dong, An Ultra-Low Frequency Parallel Connection Nonlinear Isolator for Precision Instruments, Key Engineering Materials. 257–258 (2004). https://doi.org/10.4028/www.scientific.net/kem.257-258.231.

[14] A. Carrella, M.J. Brennan, T.P. Waters, Static analysis of a passive vibration isolator with quasi-zero-stiffness characteristic, Journal of Sound and Vibration. 301 (2007) 678–689. https://doi.org/10.1016/j.jsv.2006.10.011.

[15] G. Gatti, Statics and dynamics of a nonlinear oscillator with quasi-zero stiffness behaviour for large deflections, Communications in Nonlinear Science and Numerical Simulation. 83 (2020). https://doi.org/10.1016/j.cnsns.2019.105143.

[16] A.D. Shaw, G. Gatti, P.J.P. Gonçalves, B. Tang, M.J. Brennan, Design and test of an adjustable quasi-zero stiffness device and its use to suspend masses on a multi-modal structure, Mechanical Systems and Signal Processing. 152 (2021) 107354. https://doi.org/10.1016/j.ymssp.2020.107354.

[17] N. Zhou, K. Liu, A tunable high-static-low-dynamic stiffness vibration isolator, Journal of Sound and Vibration. 329 (2010). https://doi.org/10.1016/j.jsv.2009.11.001.

[18] G. Dong, Y. Zhang, Y. Luo, S. Xie, X. Zhang, Enhanced isolation performance of a high-static–low-dynamic stiffness isolator with geometric nonlinear damping, Nonlinear Dynamics. 93 (2018).

https://doi.org/10.1007/s11071-018-4328-5.

[19] B. Yan, H. Ma, B. Jian, K. Wang, C. Wu, Nonlinear dynamics analysis of a bi-state nonlinear vibration isolator with symmetric permanent magnets, Nonlinear Dynamics. 97 (2019). https://doi.org/10.1007/s11071-019-05144-w.

[20] H. Ding, Z.Q. Lu, L.Q. Chen, Nonlinear isolation of transverse vibration of pre-pressure beams, Journal of Sound and Vibration. 442 (2019). https://doi.org/10.1016/j.jsv.2018.11.028.

[21] H. Ding, J. Ji, L.Q. Chen, Nonlinear vibration isolation for fluid-conveying pipes using quasi-zero stiffness characteristics, Mechanical Systems and Signal Processing. 121 (2019). https://doi.org/10.1016/j.ymssp.2018.11.057.

[22] H. Ding, L.Q. Chen, Nonlinear vibration of a slightly curved beam with quasi-zero-stiffness isolators, Nonlinear Dynamics. 95 (2019). https://doi.org/10.1007/s11071-018-4697-9.

[23] F.C. Moon, P.J. Holmes, A magnetoelastic strange attractor, Journal of Sound and Vibration. 65 (1979) 275–296. https://doi.org/10.1016/0022-460X(79)90520-0.

[24] D. Jordan, P. Smith, Nonlinear Ordinary Differential Equations: An Introduction for Scientists and Engineers, Oxford University Press, 2007.

[25] I. Kovacic, M.J. Brennan, The Duffing Equation: Nonlinear Oscillators and their Behaviour, John Wiley & Sons, Ltd, Chichester, UK, 2011. https://doi.org/10.1002/9780470977859.

[26] V. Gupta, M. Mittal, V. Mittal, R-peak detection based chaos analysis of ECG signal, Analog Integrated Circuits and Signal Processing. 102 (2020) 479–490. https://doi.org/10.1007/s10470-019-01556-1.

[27] V. Gupta, M. Mittal, V. Mittal, Chaos Theory and ARTFA: Emerging Tools for Interpreting ECG Signals to Diagnose Cardiac Arrhythmias, Wireless Personal Communications. 118 (2021) 3615–3646. https://doi.org/10.1007/s11277-021-08411-5.

[28] D. Anastasio, A. Fasana, L. Garibaldi, S. Marchesiello, Nonlinear Dynamics of a Duffing-Like Negative Stiffness Oscillator: Modeling and Experimental Characterization, Shock and Vibration. 2020 (2020) 1–13. https://doi.org/10.1155/2020/3593018.

[29] S. Marchesiello, L. Garibaldi, A time domain approach for identifying nonlinear vibrating structures by subspace methods, Mechanical Systems and Signal Processing. 22 (2008) 81–101. https://doi.org/10.1016/j.ymssp.2007.04.002.

[30] D. Anastasio, S. Marchesiello, Experimental Characterization of Friction in a Negative Stiffness Nonlinear Oscillator, Vibration. 3 (2020) 132–148. https://doi.org/10.3390/vibration3020011.

[31] G. Kerschen, K. Worden, A.F. Vakakis, J.C. Golinval, Past, present and future of nonlinear system identification in structural dynamics, Mechanical Systems and Signal Processing. 20 (2006) 505–592. https://doi.org/10.1016/j.ymssp.2005.04.008.

[32] J.P. Noël, G. Kerschen, Nonlinear system identification in structural dynamics: 10 more years of progress, Mechanical Systems and Signal Processing. 83 (2017) 2–35. https://doi.org/10.1016/j.ymssp.2016.07.020.

[33] F.B. Duarte, J. Tenreiro MacHado, Fractional describing function of systems with Coulomb friction, Nonlinear Dynamics. 56 (2009). https://doi.org/10.1007/s11071-008-9405-8.

[34] K. Worden, C.X. Wong, U. Parlitz, A. Hornstein, D. Engster, T. Tjahjowidodo, F. Al-Bender, D.D. Rizos, S.D. Fassois, Identification of pre-sliding and sliding friction dynamics: Grey box and black-box models, Mechanical Systems and Signal Processing. 21 (2007) 514–534. https://doi.org/10.1016/j.ymssp.2005.09.004.

[35] T. Dossogne, J.P. Noël, C. Grappasonni, G. Kerschen, B. Peeters, J. Debille, M. Vaes, J. Schoukens, Nonlinear ground vibration identification of an F-16 aircraft - Part II: Understanding nonlinear behaviour in aerospace structures using sine-sweep testing, International Forum on Aeroelasticity and Structural Dynamics, IFASD 2015. (2015) 1–19.

[36] G. Kerschen, V. Lenaerts, J.C. Golinval, VTT benchmark: Application of the restoring force surface method, Mechanical Systems and Signal Processing. 17 (2003). https://doi.org/10.1006/mssp.2002.1558.

[37] C.M. Cheng, Z.K. Peng, W.M. Zhang, G. Meng, Wavelet basis expansion-based Volterra kernel function identification through multilevel excitations, Nonlinear Dynamics. 76 (2014). https://doi.org/10.1007/s11071-013-1182-3.

[38] L. Marino, A. Cicirello, Experimental investigation of a single-degree-of-freedom system with Coulomb friction, Nonlinear Dynamics. 99 (2020). https://doi.org/10.1007/s11071-019-05443-2.

[39] L.A. Aguirre, Á.V.P. Souza, An Algorithm for Estimating Fixed Points of Dynamical Systems from Time Series, International Journal of Bifurcation and Chaos. 08 (1998) 2203–2213. https://doi.org/10.1142/S0218127498001790.

[40] J.E. Mottershead, R. Stanway, Identification of nth-power velocity damping, Journal of Sound and Vibration. 105 (1986) 309–319. https://doi.org/10.1016/0022-460X(86)90159-8.

[41] N. Jakšić, Power law damping parameter identification, Journal of Sound and Vibration. 330 (2011) 5878–5893. https://doi.org/10.1016/j.jsv.2011.07.029.